Special Topic
Forming and Heat Treatment Technologies That Support the Steel Manufacturing Process

ISIJ International, Vol. 65 (2025), No. 1, pp. 20–25
https://doi.org/10.2355/isijinternational.ISIJINT-2024-189

Short Article

Enhanced Resistance to Delayed Fracture in 0.09 mass% P-Doped High-Strength Steel Processed by Warm Tempforming

Yuuji KIMURA,[1)*] Taku MORONAGA[2)] and Kaneaki TSUZAKI[1)]

1) Research Center for Structural Materials, National Institute for Materials Science, 1-2-1 Sengen, Tsukuba, Ibaraki, 305-0047 Japan.
2) Research Network and Facility Services Division, National Institute for Materials Science, 1-2-1 Sengen, Tsukuba, Ibaraki, 305-0047 Japan.

(*Received June 18, 2024; Accepted July 19, 2024; Advance online published August 1, 2024; Published January 15, 2025*)

From the viewpoint of expanding the allowable P limit, the effect of warm tempforming on delayed fracture resistance was evaluated for 0.09% P-doped 0.4%C–1%Cr–0.7%Mn–0.2%Mo steel (mass%). The P-doped steel was warm tempformed at 500°C with a caliber-rolling reduction of 78% and annealed at 550°C for 1 h. This thermomechanical treatment created an ultrafine elongated grain structure with a strong $<110>$//rolling direction fiber texture, in which P definitely cosegregated with Mn and Mo at grain boundaries. The slow-strain-rate-test and immersion test demonstrated that warm tempforming markedly enhanced the delayed fracture resistance of the P-doped steel at a tensile strength of 1 100 MPa level, in contrast to conventional quenching and tempering treatment.

KEY WORDS: low-alloy steel; thermomechanical treatment; martensite; phosphorus segregation; hydrogen embrittlement; delayed fracture.

1. Introduction

To achieve carbon neutrality, steel scrap recycling is attracting growing attention. However, repeated recycling of steel scrap increases the contents of impurity elements such as P, S, Cu and Sn, which negatively affect the properties of steels.[1)] Therefore, in addition to reducing the impurity elements, a major challenge in steel scrap recycling is to develop manufacturing technologies that minimize the negative effects of impurity elements and further expand their allowable limits.

Although P induces intergranular embrittlement in steels, its addition offers advantages such as enhanced strength[1)] and weatherability.[2)] Hence, attempts have been made to utilize P as an alloying element through microstructure control of steels. For example, Kawakubo *et al.* reported that 0.1% C weathering steel with a P content of 0.3% (in mass%), which cannot be joined by fusion welding, could be joined through friction stir welding (FSW) process.[2)] In the stir zone, a significant decrease in ductile-to-brittle transition temperature was observed as the average ferrite grain size decreased from 23 to 2.5 μm. Min *et al.* focused on the use of P embrittlement for delamination toughening in warm tempformed 0.4%C–1%Cr–0.7%Mn–0.2%Mo steels with P contents up to 0.09%.[3)] Warm tempforming involves plastic deformation of quenched and tempered (QT) steel at elevated temperatures, and an ultrafine elongated grain (UFEG) structure with a strong <110>//rolling direction (RD) fiber texture can be obtained by warm multi-pass caliber-rolling.[4–7)] The result showed that 0.09% P-doped steel with a UFEG structure was especially toughened by delamination and exhibited superior Charpy impact property compared with QT steel with a P content of 0.001% even at subzero temperatures.

Regarding the practical application of high-strength steels, high resistance to delayed fracture is also required. Warm tempformed (TF) steels with a tensile strength, σ_B, of 1 400–1 800 MPa have been shown to exhibit superior delayed fracture properties compared to QT steels.[4–7)] However, the P contents of the TF steels were within the allowable limit of P (0.03% or less) of JIS low-alloy steels for machine structural use, such as SCM440 steel (JIS G4053: 2023). It is well known that in QT steels, P facilitates hydrogen embrittlement.[8,9)] Therefore, from the viewpoint of expanding the allowable P limit, we studied the effect of warm tempforming on delayed fracture resistance for 0.09% P-doped steel.

2. Experimental Procedure

0.4%C–1%Cr–0.7%Mn–0.2%Mo steels containing 0.001 and 0.09% P, which are similar in basic chemical composi-

* Corresponding author: E-mail: KIMURA.Yuuji@nims.go.jp

tion to JIS-SCM440 steel, were prepared by 100 kg vacuum induction melting and casting. **Table 1** lists the chemical compositions of 0.001% P (LP) and 0.09% P (HP) steels. The HP steel was oil-quenched after austenitizing at 920°C for 1 h, warm tempformed at 500°C using caliber-rolling with a cumulative reduction of 78% and annealed at 550°C for 1 h (HP_{TF}). For reference, normalized bars were austenitized at 920°C for 1 h, oil-quenched, and tempered at 550°C for 1 h. The average prior-austenite grain size of the QT samples was approximately 30 μm, regardless of the P content. Details of the material preparations were described elsewhere.[3] As shown in **Table 2**, the σ_B of LP_{QT}, HP_{QT} and HP_{TF} is comparable at approximately 1 100 MPa.

Microstructures and fracture surfaces were observed by field emission scanning electron microscopy (FE-SEM). Crystallographic orientation was analyzed using an electron backscatter diffraction (EBSD) detector installed in a FE-SEM, with a step size of 50 nm. Elemental analysis was performed using energy-dispersive X-ray spectrometer (EDS) in scanning transmission electron microscope (STEM) (JEM-ARM300F). The thin film sample for STEM was prepared with a focused ion beam (FIB).

Slow-strain-rate testing (SSRT) was performed for notched bar specimens with a stress concentration factor of 4.9 (see Fig. S1(a)).[4–7] Hydrogen was introduced homogeneously into the specimens by cathodic charging with a 0.1 N NaOH aqueous solution or a 3%NaCl + 0.3%NH_4SCN aqueous solution at current densities of 0.2–10 A/m^2 for 168 h. The hydrogen-charged specimens were tensioned at a crosshead speed of 1 mm/min to a nominal stress of 230 or 920 MPa at the notch and tensioned at a crosshead speed of 0.005 mm/min to failure. The purpose of tensile loading before SSRT was to shorten the testing time and minimize hydrogen release during SSRT. Notch tensile strength, σ_{NB}, was calculated by dividing the maximum load by the cross-sectional area at the notch. In the QT sample of LP_2 steel with a σ_B of 1 290 MPa, the relationship between σ_{NB} and diffusible hydrogen (H_D) content in this SSRT condition was almost the same as that in SSRT for Cd-plated specimens (see Fig. S1(b)).

Table 1. Chemical compositions of low P (LP) and high P (HP) steels (mass%). For LP steel, LP_2 steel was used to interpolate the data sets from LP_1 steel in Figs. 3 and 4.

Steels	C	Si	Mn	Cr	Mo	P	S
LP_1	0.40	0.24	0.73	1.04	0.22	0.001	<0.001
LP_2	0.41	0.25	0.69	1.02	0.20	0.001	<0.001
HP	0.41	0.24	0.71	1.00	0.20	0.093	0.0005

Table 2. Tensile properties of QT and TF samples; yield strength, $\sigma_{0.2}$, tensile strength, σ_B, uniform elongation (UEL), total elongation (TEL), and reduction in area (RA).

Samples	$\sigma_{0.2}$ (MPa)	σ_B (MPa)	UEL (%)	TEL (%)	RA (%)
LP_{1QT}	999	1 122	5.4	15.6	60
LP_{2QT}	1 002	1 112	5.5	14.5	57
HP_{QT}	993	1 137	6.1	13.2	46
HP_{TF}	1 059	1 133	7.9	16.6	52

An immersion test was conducted for cylindrical specimens (7×20 mm) at 30°C with a 0.5 mol/L NaCl + 0.01 mol/L HCl aqueous solution (pH=2), simulating the atmospheric corrosive environment in Okinawa.[10] Thermal desorption spectrometry (TDS) analysis was conducted to measure the H_D content; hydrogen that desorbed up to 300°C during TDS was defined as H_D. Apparent activation energy for hydrogen desorption, E_a, was evaluated by Kissinger plots of the hydrogen desorption peak temperature, T_C, in TDS at different heating rates, Φ, of 100–300°C[11] for the plate specimens (1×5×15 mm); hydrogen charging was performed using a 0.1 N NaOH aqueous solution at a current density of 25 A/m^2 for 48 h to saturate the specimens with hydrogen.[6,7]

3. Results and Discussion

Figure 1 shows a UFEG structure with a strong <110>//RD fiber texture in HP_{TF}. The UFEG structure consisted of ribbon- and rod-shaped grains, which inherited the hierarchical heterogeneity of the tempered martensitic structure consisting of blocks and packets within prior-austenite grains. The average transverse intercept length was measured to be 0.5 μm for high angle grain boundaries (HAGBs) with a misorientation angle of 15° or more. Cementite particles

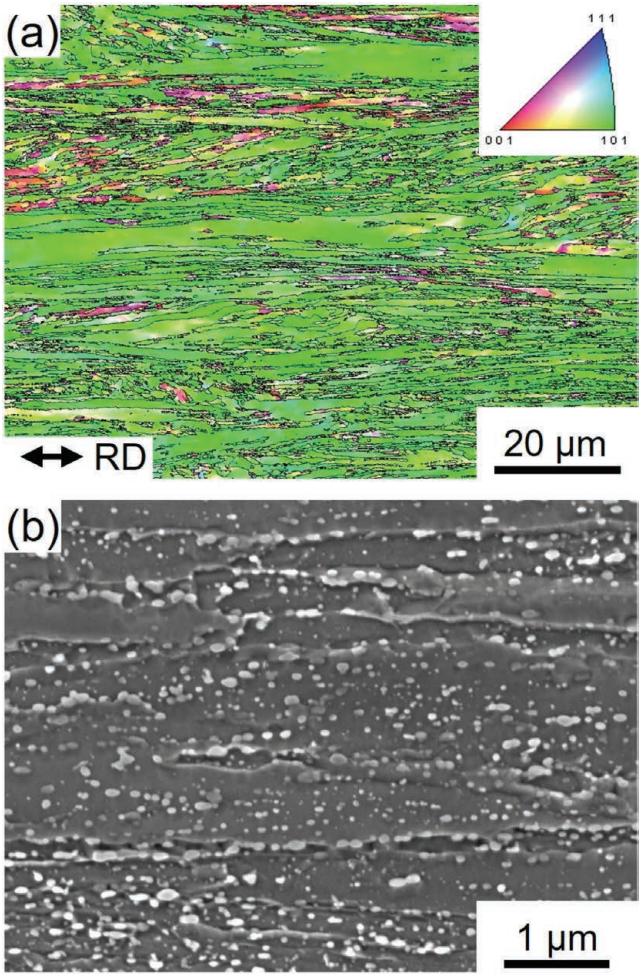

Fig. 1. Inverse pole figure (IPF) map for the RD (a) and FE-SEM image (b) showing a UFEG structure with a strong <110>//RD fiber texture in HP_{TF}. Black lines in (a) are HAGBs with a misorientation angle of 15° or more. (Online version in color.)

were aligned in the RD and more spherical compared to those in LP_{QT} and HP_{QT}.[3] **Figure 2** presents the results of the STEM-EDS analysis in the UFEG structure. As expected, Cr, Mn, and Mo partitioned into cementite particles. Elemental mapping further revealed that P and S, as well as Mo and Mn, segregated at the HAGB. Depletion zones of Cr and Mn were also observed around the HAGB. The elemental line profile indicated that the element concentration at the grain boundaries (GBs) was in the order of P<Cr<Mn<Mo; however, S concentration could not be quantified because S-K_α peak (2.31 keV) overlapped with Mo-L_α peak (2.29 keV). Regarding the cosegregation of P and these elements, Morita[12] showed by a first-principles calculations on Fe Σ3(111) GB that Cr, Mn, and Mo exhibited repulsive interactions with P at GB and reduce the GB segregation of P. The first-principles calculations by Ito *et al.*[13] also showed that Mo segregation at Fe Σ3(111) GB significantly reduced the GB segregation of H due to repulsive interactions between H and Mo. Furthermore, Mo is a strong cohesion enhancer.[14] Hence, Mo may suppress intergranular embrittlement in the present steel.

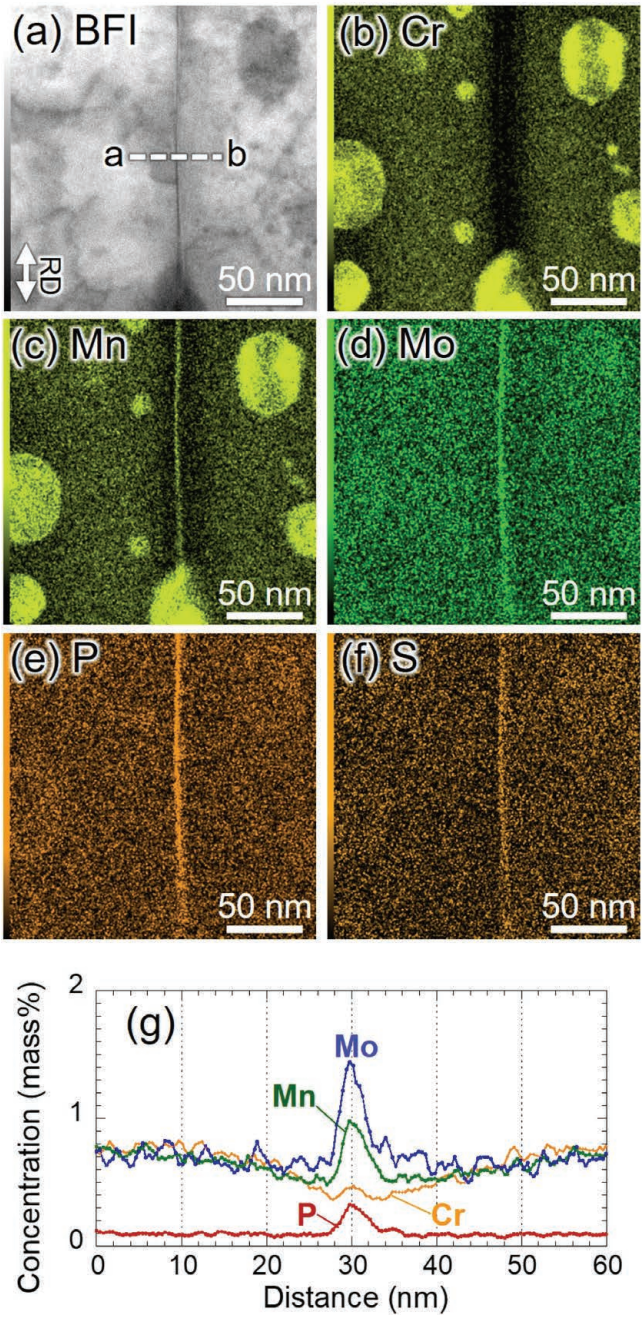

Fig. 2. STEM bright field image (a), STEM-EDS elemental maps of Cr (b), Mn (c), Mo (d), P (e), S (f), and elemental line profiles along the broken line ab across a HAGB (g) for HP_{TF}. (Online version in color.)

Figure 3 shows the results of the immersion test to determine the maximum absorbed H_D content, H_E, in an atmospheric corrosive environment. Note that the rust layers for LP_{QT} were removed by sandblasting because they could not be removed by ultrasonic cleaning as for HP_{QT} and HP_{TF}. In all samples, the H_D content reached nearly a constant value after the immersion test for 120 h or longer. H_E values were thus determined to be 0.06 mass ppm for HP_{QT}, 0.09 mass ppm for HP_{TF}, and 0.13 mass ppm for LP_{QT}. Although the H_E of LP_{QT} was higher than that of HP_{QT} and HP_{TF}, it was as low as that for QT steels without effective hydrogen trapping sites[4–7,11] such as nanometer-sized V-carbides[15] and Mo-rich precipitates.[5,7] **Table 3** lists the E_a values. From the TDS analysis, E_a was estimated to be 15.3 kJ/mol for

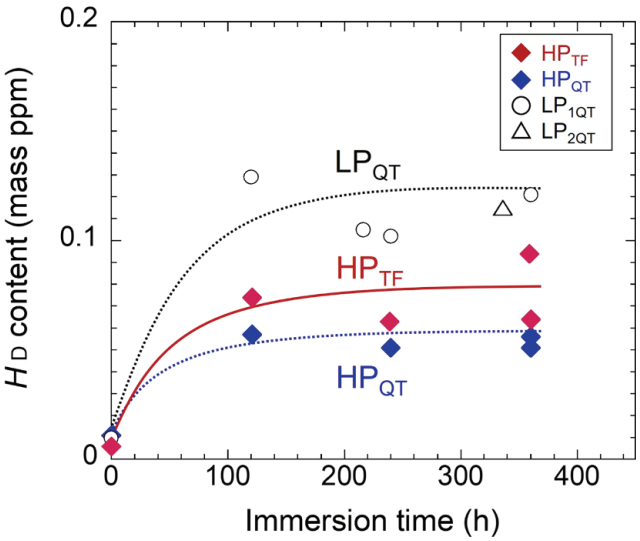

Fig. 3. Change in H_D content as a function of immersion time. The immersion test was conducted at 30°C with a 0.5 mol/L NaCl + 0.01 mol/L HCl aqueous solution (pH=2), simulating the atmospheric corrosive environment in Okinawa.[10] (Online version in color.)

Table 3. E_a values for various steels. 0.6%C-2%S-1%Cr steel was quenched and tempered at 500°C for 1 h (QT) and warm tempformed at 500°C (TF).[4] E_a values for cold drawn and recrystallized pure irons are shown for the strain field of dislocations and GBs, respectively.[11]

Samples	E_a (kJ/mol)
LP_{QT}	18.9
HP_{QT}	15.3
HP_{TF}	13.3
0.6%C-2%Si-1%Cr QT steel[4]	19.4
0.6%C-2%Si-1%Cr TF steel[4]	16.5
Cold drawn pure iron[11]	26.8
Recrystallized pure iron[11]	17.2

HP_{QT}, 13.3 kJ/mol for HP_{TF}, and 18.9 kJ/mol for LP_{QT} (see Fig. S2). The comparison of these E_a values with those for other steels[4–7,11] suggests that hydrogen might be reversibly trapped in αFe grain boundaries, αFe/Fe_3C interfaces and dislocation strain fields in these samples, as previously discussed in 0.6%C-2%Si-1%Cr QT and TF steels.[4] The hydrogen trapping ability of HP_{QT} and HP_{TF} was slightly weaker than that of LP_{QT}.

Figure 4 shows the change in σ_{NB} as a function of H_D content. SSRT from 920 MPa was performed under the hydrogen-precharged condition where σ_{NB} exceeded 1 000 MPa in SSRT from 230 MPa. There was no significant difference in hydrogen degradation between SSRT from 230 and that from 920 MPa, indicating that hydrogen release during SSRT from 230 MPa was not significant. In the hydrogen-uncharged state, σ_{NB} of the QT samples deteriorated from 1 840 to 1 690 MPa by the addition of 0.09% P but improved to 1 890 MPa by warm tempforming. On the other hand, hydrogen charging degraded σ_{NB} in all samples. The σ_{NB} decreased significantly in the low- H_D content range of ~1 mass ppm, followed by a gradual decrease. However, when compared at the same H_D content, the decrement in σ_{NB} was in the order of HP_{TF}<LP_{QT}<HP_{QT}, indicating that hydrogen embrittlement susceptibility was in the order of HP_{TF}<LP_{QT}<HP_{QT}. It should be noted that HP_{TF} retained a high σ_{NB} above 1 000 MPa even with a high- H_D content of around 3 mass ppm, where the σ_{NB} for LP_{QT} sample dropped to around 500 MPa.

Delayed fracture resistance under atmospheric corrosive environments has been discussed in terms of the balance between H_E and the critical H_D content, H_C, for hydrogen embrittlement.[4–7,15,16] Here, the relationship between σ_{NB} and H_D content can be approximated by the power-law relationship shown in Fig. 4, to determine H_C at a given applied stress, σ_a. **Table 4** lists the H_C and H_E values. When σ_a was $0.9\sigma_B$, H_C was calculated to be 0.73 mass ppm for LP_{QT}, 0.16 mass ppm for HP_{QT} and 3.7 mass ppm for HP_{TF}.

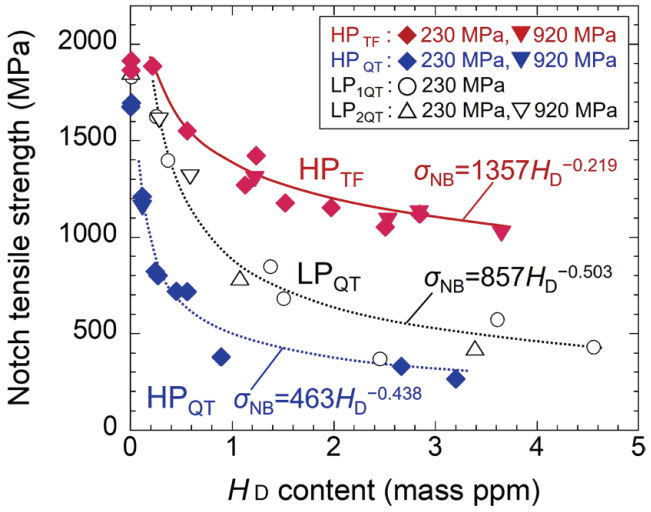

Fig. 4. Change in σ_{NB} as a function of H_D content with SSRT from an initial tensile stress of 230 or 920 MPa. In all samples, hydrogen was introduced by cathodic charging at current densities of 0.2–10 A/m^2 for 168 h with a 0.1 N NaOH aqueous solution (H_D content < 0.3 mass ppm) or a 3%NaCl + 0.3%NH_4SCN aqueous solution (H_D content > 0.3 mass ppm). (Online version in color.)

The H_C/H_E value was thus calculated to be 5.6 for LP_{QT}, 2.7 for HP_{QT}, and 41 for HP_{TF}. H_C/H_E of HP_{QT} was between that of 0.2%C–1%Mn–0.002%B (=3.6) and JIS-SCM435 (=2.1) steels,[16] which were QT steels with respective σ_B of 1 305 and 1 320 MPa; 1 300 MPa-grade bolts of these steels suffered delayed fracture during outdoor exposure tests in Tsukuba and Okinawa. On the other hand, H_C/H_E of LP_{QT} was close to that of 0.2%C–1%Mn–0.002%B QT steel (=6.7) with a σ_B of 1 050 MPa,[16] where no delayed fracture occurred in the outdoor exposure tests of the bolts. As for HP_{TF}, its H_C/H_E was much larger than that of LP_{QT} and was 7.0 even at a σ_a of 1 500 MPa. Therefore, it can be concluded that the delayed fracture resistance of HP steel is markedly improved by warm tempforming, in addition to Charpy impact property.[3]

Figure 5 shows fractographs from the SSRT specimens for LP_{QT} and HP_{QT}. Almost 100% of the fracture surfaces of HP_{QT} consisted of intergranular fracture along prior-austenite GBs, regardless of the H_D content. However, in the hydrogen-charged specimen, an uneven fracture surface suggested that intergranular fracture occurred more frequently (Fig. 5(e)). From a first-principles calculations Yamaguchi *et al.*[17] indicated that the combined mobile and immobile effects of hydrogen largely reduced GB cohesive energy (70–80% reduction), compared to the sole immobile effect of hydrogen (10–20% reduction). As shown in Fig. 4, the decrement in σ_{NB} is much larger in hydrogen than in phosphorus. This may be due to the contribution of the mobile effect of hydrogen on intergranular decohesion. Although not shown in Fig. 5, the uncharged specimen for LP_{QT} failed in a completely ductile manner. As the H_D content increased, the predominant fracture mode changed from microvoid coalescence to quasicleavage (Figs. 5(c), 5(d)). Furthermore, intergranular fracture was observed in the high- H_D content range where its σ_{NB} dropped to around 500 MPa (Figs. 5(g), 5(h)). These findings demonstrate that P facilitates hydrogen-induced intergranular fracture.

Figure 6 shows fractographs from the SSRT specimens for HP_{TF}. Macroscopic fracture modes of HP_{TF} were characterized by delamination in the RD and shear fracture, and the frequency of delamination was more pronounced with hydrogen charging. The shear fracture progressed by microvoid coalescence even with a high- H_D content of around 3 mass ppm (Fig. 6(h)). By contrast, the predominant mode of delamination in the uncharged specimen was quasicleav-

Table 4. Critical H_D content under an applied stress of $0.9\sigma_B$, H_C, and maximum absorbed H_D content in an atmospheric corrosive environment, H_E, for LP_{QT}, HP_{QT}, HP_{TF}, 0.2%C–1%Mn–0.002%B (A11, A13),[16] and JIS-SCM435 (B13)[16] steels.

Samples	σ_B (MPa)	H_C (ppm)	H_E (ppm)	H_C/H_E
LP_{QT}	1 117	0.73	0.13	5.6
HP_{QT}	1 137	0.16	0.06	2.7
HP_{TF}	1 133	3.7	0.09	41
A11[16]	1 050	1.0	0.15	6.7
A13[16]	1 305	0.58	0.16	3.6
B13[16]	1 320	0.25	0.12	2.1

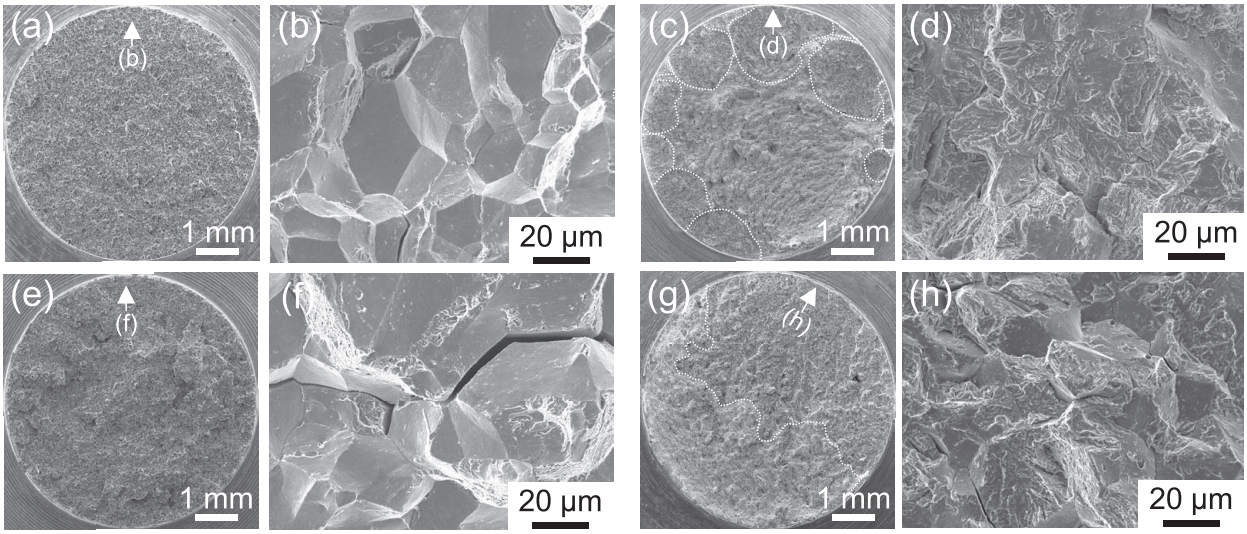

Fig. 5. Fracture surfaces of the SSRT specimens for HP_{QT} with H_D contents of 0 mass ppm (a, b) and 3.2 mass ppm (e, f), and LP_{QT} with H_D contents of 1.4 mass ppm (c, d), and 2.5 mass ppm (g, h).

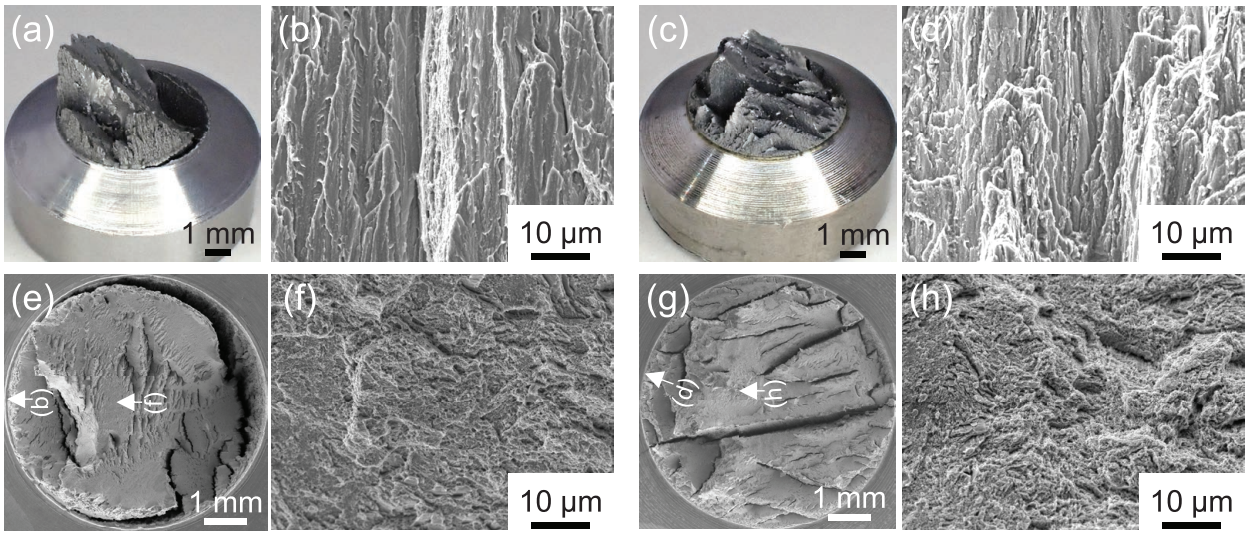

Fig. 6. Fracture surfaces of the SSRT specimens for HP_{TF} with H_D contents of 0 mass ppm (a, b, e, f), and 2.5 mass ppm (c, d, g, h). (Online version in color.)

age (Fig. 6 (b)), which appeared to change to intergranular fracture along UFEG boundaries with hydrogen charging (Fig. 6(d)). **Figure 7** shows delamination cracks that preferentially propagated along UFEG boundaries. Hence, the σ_{NB} for HP_{TF} is considered to largely depend on the occurrence of delamination, as discussed for other TF steels with UFEG structures.[4–7)]

Possible mechanisms by which hydrogen embrittlement resistance is enhanced by warm tempforming are as follows. Firstly, intergranular fracture along prior-austenite GBs is suppressed in the transverse direction.[4–7)] Secondly, the UFEG structure with a strong <110>//RD fiber texture provides more ductile and tougher planes normal to the RD whereas weaker GBs and planes along the RD. This further suppresses transverse brittle cracking and creates the conditions for delamination under a triaxial tension state that generates near the notch root.[7)] Although delamination cracking lowers the σ_{NB}, it relaxes the triaxial tension state and mitigates hydrogen accumulation. Thirdly, multiple microcracks along the RD near the notch root or crack tip might reduce the driving force for the main crack propagation through the stress-shielding effect associated with the interference of multiple microcracks.[7)] As shown in Fig. 2, the GB segregation of P further facilitates the hydrogen-assisted delamination cracking and microcracks along the RD. The synergistic effect of these mechanisms is thus considered to suppress brittle main crack propagation and maintain a high σ_{NB} above 1 000 MPa or over even at a high- H_D content of 3 mass ppm in HP_{TF}. Similar hydrogen embrittlement behavior has been observed in 0.37%C–0.9%Mn–0.002%B TF steels (σ_B = 1 400 MPa),[6)] and cold caliber-rolled pearlitic 0.6%C–2%Si–1%Cr steel (σ_B = 1 670 MPa).[18)] On the other hand, the σ_{NB} of 0.6%C–2%Si–1%Cr TF steel (σ_B = 1 540 MPa) dropped to 600 MPa at high- H_D content of 3 mass ppm,[4)] even though it has a hydrogen trapping ability similar to HP_{TF}. This may be explained in terms of differences in the occurrence of hydrogen-assisted delamination fracture in the UFEG structures with various GB characters. Clarification of this requires a more detailed investigation considering the GB characters of the UFEG structure.

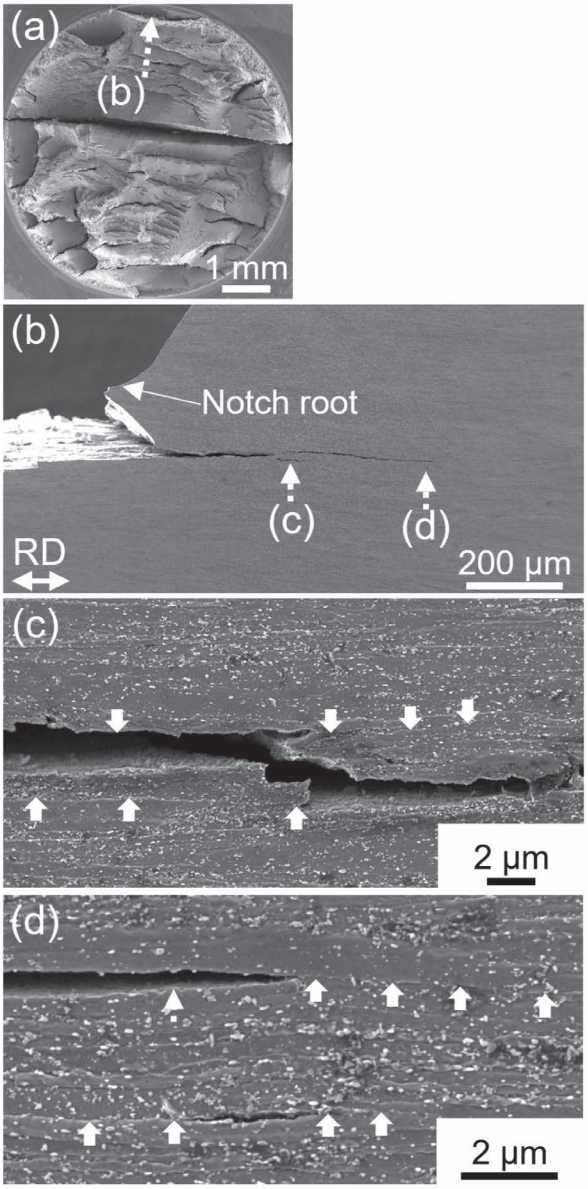

Fig. 7. Relationship between microstructure and delamination crack path for HP_{TF} with H_D content of 2.8 mass ppm. Arrows in (c, d) indicate the UFEG boundaries.

4. Summary

Warm tempforming effect on delayed fracture resistance was evaluated for 0.09% P-doped steel at a σ_B of 1 100 MPa level. Warm tempforming combined with annealing at 550°C for 1 h evolved a UFEG structure with a strong <110>//RD fiber texture, in which P definitely cosegregated with Mn, and Mo at GBs. In quenching and tempering at 550°C for 1 h, the addition of 0.09% P significantly degraded hydrogen embrittlement resistance for the steel by facilitating intergranular fracture along prior-austenite GBs. By contrast, warm tempforming markedly enhanced the hydrogen embrittlement resistance of the P-doped steel due to the UFEG structure. The TF steel was shown to have a significantly high delayed fracture resistance when considering the balance between the critical H_D content for hydrogen embrittlement and the maximum absorbed H_D content in an atmospheric corrosive environment. This fact indicates that an impurity element of P can be utilized as an effective element against hydrogen embrittlement if we correctly chose the microstructure.

Supporting Information

[Figs. S1–S2] This material is available on the Journal website at https://doi.org/10.2355/isijinternational.ISIJINT-2024-189.

Conflict of Interest Statement

The authors declare no conflicts of interest.

Acknowledgments

The authors thank Mr. Iida, Mr. Kobayashi and Mr. Hibaru for materials processing with caliber rolling, and Ms. Seki for her help with TDS analysis and FE-SEM observation. A part of this study was supported by the Electron Microscopy Unit, NIMS. This study was partly supported by grants from the JSPS KAKENHI Grant Number 24K01204, and MEXT Program: Data Creation and Utilization Type Material Research and Development Project Grant Number JPMXP1122684766.

REFERENCES

1) I. Daigo, K. Tajima, H. Hayashi, D. Panasiuk, K. Takeyama, H. Ono, Y. Kobayashi, K. Nakajima and T. Hoshino: *ISIJ Int.*, **61** (2021), 498. https://doi.org/10.2355/isijinternational.ISIJINT-2020-377
2) T. Kawakubo, T. Nagira, K. Ushioda and H. Fujii: *ISIJ Int.*, **61** (2021), 2150. https://doi.org/10.2355/isijinternational.ISIJINT-2021-007
3) X. Min, Y. Kimura, T. Kimura and K. Tsuzaki: *Mater. Sci. Eng. A*, **649** (2016), 135. https://doi.org/10.1016/j.msea.2015.09.102
4) Y. Nie, Y. Kimura, T. Inoue, F. Yin, E. Akiyama and K. Tsuzaki: *Metall. Mater. Trans. A*, **43A** (2012), 1670. https://doi.org/10.1007/s11661-011-0974-7
5) Y. Kimura, T. Inoue and E. Akiyama: *Mater. Sci. Eng. A*, **703** (2017), 503. https://doi.org/10.1016/j.msea.2017.07.091
6) Y. Kimura, T. Inoue, T. Otani, A. Ochiai, S. Ikurumi and T. Takatsuji: *Mater. Sci. Eng. A*, **819** (2021), 141514. https://doi.org/10.1016/j.msea.2021.141514
7) Y. Kimura, T. Moronaga and T. Inoue: *ISIJ Int.*, **62** (2022), 377. https://doi.org/10.2355/isijinternational.ISIJINT-2021-407
8) J. Kameda and C. J. McMahon, Jr.: *Metall. Trans. A*, **14A** (1983), 903. https://doi.org/10.1007/BF02644295
9) S. Komazazki, S. Watanabe and T. Misawa: *ISIJ Int.*, **43** (2003), 1851. https://doi.org/10.2355/isijinternational.43.1851
10) K. Matsuoka, N. Uno, E. Akiyama, Y. Hagihara, S. Matsuyama and H. Harada: *Steel Constr. Eng*, **20** (2013), 29 (in Japanese). https://doi.org/10.11273/jssc.20.79_29
11) W. Y. Choo and J. Y. Lee: *Metall. Trans. A*, **13A** (1982), 135. https://doi.org/10.1007/BF02642424
12) S. Morita: *Kobelco Tech. Rev.*, **40** (2023), 1.
13) K. Ito, Y. Tanaka, K. Tsutsui and T. Omura: *Comput. Mater. Sci.*, **218** (2023), 111951. https://doi.org/10.1016/j.commatsci.2022.111951
14) W. T. Geng, A. J. Freeman, R. Wu and G. B. Olson: *Phys. Rev. B*, **62** (2000), 6208. https://doi.org/10.1103/PhysRevB.62.6208
15) S. Yamasaki and T. Takahashi: *Tetsu-to-Hagané*, **83** (1997), 454 (in Japanese). https://doi.org/10.2355/tetsutohagane1955.83.7_454
16) E. Akiyama: *ISIJ Int.*, **52** (2012), 307. https://doi.org/10.2355/isijinternational.52.307
17) M. Yamaguchi, J. Kameda, K. Ebihara, M. Itakura and H. Kaburaki: *Philos.Mag.*, **92** (2012), 1349. https://doi.org/10.1080/14786435.2011.645077
18) R. Ueji, Y. Kimura and T. Inoue: *ISIJ Int.*, **62** (2022), 368. https://doi.org/10.2355/isijinternational.ISIJINT-2021-429